Liu Albert Tianxiang (Orcid ID: 0000-0001-8854-5854)

Temporally Resolved Concentration Profiling via Computationally Limited, Distributed Sensor Nodes

Matthew Lee Manion[1], Joshua Doctor[2], Albert Tianxiang Liu[1,3*]

[1] Department of Chemical Engineering, University of Michigan, Ann Arbor, MI 48105

[2] Department of Electrical Engineering, University of Michigan, Ann Arbor, MI 48105

[3] Department of Material Science and Engineering, University of Michigan, Ann Arbor, MI 48105

[*] Corresponding Author Email: atliu@umich.edu

Abstract:

Accurate mapping of chemical concentrations in reactor networks remains an obstacle to establish complete systems-level insight and control. This issue extends beyond traditional reactor design to biological and other inaccessible systems of interest. Recent developments in novel materials with non-volatile memory allow autonomous sensor nodes to record information with minimal external supervision. Integrating these materials in solution suspended particles demonstrates the unique potential for diffuse measurements of chemical data at the microscale. In this study, we establish a generalized workflow for the simulated deployment of time aware particle sensors (TAPS) in ideal reactor systems to measure analyte profiles, using Gillespie kinetic Monte Carlo algorithms (KMC). Our results show that computationally-limited, chemically sensitive tracer particles capable of timestamping an analyte detection event can provide accurate analyte profiles throughout multi-stage reactors in an ensemble fashion.

Topic Heading

Reaction Engineering, Kinetics, and Catalysis; Particle Technology & Fluidization

Keywords

sensor, memristor, simulation, colloids, reaction

Introduction

This is the author manuscript accepted for publication and has undergone full peer review but has not been through the copyediting, typesetting, pagination and proofreading process, which may lead to differences between this version and the Version of Record. Please cite this article as doi: 10.1002/aic.18691

This article is protected by copyright. All rights reserved.

Author Manuscript

Author Manuscript

Over a century since its inception, chemical engineering still seeks methods for complete control and concentration mapping inside reactor systems[1]. Traditional reactor analysis (and its constituent mass, energy, and momentum balances) serves well as an academic tool and modeling basis for many practical applications[2]. In real reactors and complex systems that differ from idealities, empirical fitting is often necessary[3–7]. In industrial settings, there are an array of apparatus to monitor an evolving chemical system and generate the empirical data necessary for reactor modeling[8,9]. Fixed, integrated sensors (typically electrochemical or optical) and analytical sampling techniques (*e.g.*, gas and liquid chromatography coupled with mass spectrometry) are used to provide temporal readings or precise characterization of chemical data in reactor systems. Outside the realm of industry, the human body represents a good example of a complex system with thousands of potential analytes whose concentrations are associated with health outlook and disease prognosis[10]. Implanted sensors for blood glucose and *ex vivo* blood metabolite assays are analogous ways chemical engineers can study and understand biochemical processes[11–14]. Complete spatial concentration mapping, in the case of both man and machine, would require regularly interspersed sensor nodes to take aggregate measurements. While feasible for industrial process equipment, installing many sensors into people would certainly be undesirable. Recently, untethered, self-sufficient sensor nodes that traverse within a system of interest and continuously sample analyte have been proposed as an alternative for reactor-level spatial profiling[15]. Since the path the sensor takes is not fixed, it is not guaranteed to sample representative volumes in the system; thus, releasing multiple sensors in a swarm or network is prudent for accurate temporal and spatial mapping.

Sensor networks, as seen for decades, consist of meso- to macro-scale nodes that often have fixed positions, and they mainly serve to take aggregated measurements of large spaces[16–18].

Author Manuscript

These networks use conventional integrated circuit (IC)-chip control systems with adequate access to computation and faculties to maintain signal fidelity. Further, scaled down IC-chips for encapsulated, mobile sensors to wear or implant have become quite sophisticated[19–28]. For the purposes of this article, we will define such a sensor as a "point" sensor, which means that a single point/node has enough access to computation that one sensor can generate an entire temporal or spatial profile (**Supplemental Figure S1a**). By releasing many sensors, confidence intervals can be established with parallel readings and ideal mappings are achieved. One pertinent example of a "point" sensor to highlight, by De la Paz *et al.*[21], shows pros and cons of downsizing IC sensing platforms; in this case, for an ingestible pill that traverses the intestinal tract *in vivo* and reports instantaneous glucose concentration. Adequate access to computation allows the sensor's response to be calculated and transcribed/transmitted *in situ*, but computation extent and complexity are held back by power requirements at the meso to micro-scale transition[18,29,30]. The example mentioned above minimized sensor size by removing a power supply and utilizing a clever scheme for *in situ* energy generation, but the size of the pill is still on the order of cm[21]. If an aggregated measurement scheme and multiple IC-based sensors were used, the complex device assembly, calibration, as well as the large combined system size would ultimately hinder their wide-spread adaptation for analyte profiling in people and other flow-based reactor systems[3,31]. For other remote and traditionally inaccessible environments, many sensors are likely needed to confidently map the search space (**Supplemental S1d)** and maintain a buffer to allow some sensors to fail or become trapped[32,33]. Distributed, autonomous measurement systems should thus be small, cheap, and easy to fabricate. These design stipulations push an IC framework further away from niche feasibility and anticipate next generation sensing technologies based on analog computation and material memory (rather than digital storage) can simultaneously overcome the manufacturing,

length scale, power, and data storage challenges while providing temporal/spatial mapping capability.

The future of intelligent sensor systems is closely linked to the development of novel electronic materials. Colloidal robots are of a length scale (1-100 μm) where access to conventional computation is highly limited, and task-first design principles are complicated by the lack of viable control systems[29,30,34,35]. As a trade-off, their compact size and solution suspended nature confer these colloidal machines the inherent mobility to enter otherwise inaccessible environments[29,35–38], and sample enclosed spaces along highly stochastic paths[15,36,39]. External fields can be imposed on such particles to control their movement[36,40]; however, applications with high communication signal impedance necessitate the use of unsupervised colloidal robots that possess energy autonomy, as well as efficient on-board information processing and storage capabilities[30,41,42].

Memory resistive (or memristive) materials, whose intrinsic conductivity is modulated by the net motion of charges, form the basis of an energy efficient computation platform called in-memory computing[43,44]. This relatively new computation scheme, unlike the classical von Neumann architecture, allows logical and memory functions to occupy the same space, with no additional power required to transmit or store that data locally[39,43]. Memristive devices have been fabricated for over a decade, with techniques approaching real-world practicality[43]. Previous simulation work on memristor-based colloidal robotics has established a framework to pursue distributed information gathering in a variety of important systems[15,39]. This framework relies on analog time-keeping mechanisms via the implementation of a basic memristive circuit (consisting of a voltage source, a fixed/variable resistor, and a memristor) and duplicating it into a one-dimensional (1-D) array of parallel memristive elements (**Supplemental Figure S1c.i)**. The constant voltage source across the 1-D array drives electron flow from one memristive block to

Author Manuscript

the next in a predictive and temporally defined manner[39]. This simple circuit is capable of analog time keeping and has been shown to act similarly to inert tracers in elucidating residence times in reactor systems[15,39]. These memristor-based tracers process information in a completely autonomous and self-sufficient fashion that requires no external control or supervision[15,39].

This work builds on the concept of a simple time-keeping mechanism in the 1-D memristor array and investigates the potential of generalized time-aware colloidal particles. When memristor arrays are equipped with chemical sensing capabilities, they can extract useful concentration information in isolated systems with no energy required to store the information. We call a general version of these colloidal tracers, with simultaneous sensing and time-keeping mechanisms, "time-aware particulate sensors" or "TAPS", for short. Individually, these TAPS are capable of recording the onset time of a chemical detection event[39]. When deployed as a collective, we use TAPS to profile the analyte concentrations throughout an entire reactor system by comparing their ensemble sensing times (**Supplemental Figure S1a**). We define such a sensor as "distributed", meaning a single sensor node can only generate a small piece of information and access to computation is limited and "distributed" among all sensors. In our case, this single piece of information is when individual TAPS encounter enough analyte to "react". In our analogous example, this would stop current flow in a 1-D chemi-memristive circuit. It is only when these sensors are deployed in swarms or ensembles that statistical measurement profiles can be elucidated. In this work, we demonstrate the capability of computationally limited sensor swarms to map temporal concentration profiles in reactor systems over long simulated time scales. This was previously believed to be a capability unique to IC based microelectronic devices, which suffer from fabrication complexity and energy constraints for continued downscaling[35]. We show that while sensor consumption (or shut off) follows sigmoidal behavior predicted by kinetics, accuracy is

Author Manuscript

Author Manuscript

nonlinearly associated with sensor consumption via a second-order behavior and characterized by an optimum. Further, we highlight the distributed sensors' ability to map dynamic concentration profiles, with better accuracy outcomes in scenarios where analyte number concentration decreases as a function of sensor consumption. We examine model inputs for their sensitivity and effect on accuracy (with sensor detection kinetics and the number of sensors playing key roles), and demonstrate that sensor parameters for multi-compartment reactor systems can be optimized using *a priori* estimates of the residence time distributions (RTDs). It is important to note that 1-D memristor arrays are only used as an example for time-keeping in the present study. The time-aware, sensing-recording scheme for distributed sensor nodes established here is not limited to memristor materials and is broadly applicable to any microscale sensors with the ability to timestamp rare events[45–49].

Methods

Simulation Approach

Sensing simulations typically focus on only surface adsorption interactions, as the concentration information can be converted to a calibrated output and stored/transmitted with adequate access to energy and computation[50,51]. The measured response is only a function of the sensing surface properties in this case. However, distributed TAPS in the colloidal regime require additional kinetic considerations (**Supplemental Figure S1b**). The particles can only map a system properly if they are well mixed. Since TAPS are sized within 10× to biological cells, it is assumed here they can be well mixed in the system at a molecular level. Accuracy in the TAPS system is dependent on a high percentage of the collective particles reacting in a cohesive manner. If some particles are kinetically biased (*i.e.,* entrapment, channeling) to sample areas of high/low analyte, it will skew the collected data and misrepresent the profile. In this case, it is pertinent to

simulate the collision or "reaction" between TAPS and the analyte. To simulate long timescales, kinetic Monte Carlo (KMC) simulations were used over molecular dynamics for computational tractability. Monte Carlo simulations don't take into account local positions or trajectories of the particles or analytes, and it is reliant on kinetic rate parameters being known for the reaction of interest[52].

Monte Carlo Algorithm & Materials

The simplest Monte Carlo method for simulating chemical reactions is the direct Gillespie method, which uses pseudo-random numbers to calculate when, and which, reactions happen[53]. The physics based variable a_j represents the individual propensity for reaction j (R_j) to occur

$$\Delta \square = \frac{1}{\sum_{\square} \square_{\square}(\square)} \square\square\square_{10}\left(\frac{1}{\square_1}\right) \tag{1}$$

$$\sum_{\square}^{\square} \square_{\square}(\square) > \square_2 \sum_{\square} \square_{\square}(\square) \tag{2}$$

at an instantaneous point in time, and is based on an elementary reaction rate equation. As a note, all logarithmic functions referenced in this work are base 10 and denoted as log. The direct Gillespie method calculates the time step, Δt, until a reaction happens as a function of a_j and a pseudorandom, fractional number r_1 for every iteration (**Equation 1**). This can suffer from high computational cost, but it is the most physically correct Gillespie method[54]. It also calculates which reaction happens in that Δt by finding which cumulative reaction propensity index j exceeds the total propensity over all j multiplied by some random fraction r_2 (**Equation 2**). Modifications to the original have since been made, and the approximate tau-leaping or adaptive tau-leaping methods offer a good trade-off between computational time and precision (**Equation 3**)[54].

Author Manuscript

$$\square(\square + \square\square) = \square(\square) + \square(\square\square\square'(\square)) \quad (3)$$

Our simulation utilizes the approximate tau-leaping Gillespie method to generate reaction data for TAPS. Tau-leaping assumes that the variable of interest, number of active sensors x, changes in time as a Poisson distributed variable P, with an average $\lambda = \Delta t x'(t)$ of the individual reaction propensity a_j. $P(\Delta tx'(t))$ calculates the number of reaction events that occurred in time Δt, and thus is approximating the original (direct) Gillespie algorithm. The assumptions necessary for tau-leaping hold so long as the system is well mixed and the reaction propensities do not change substantially inside the Δt time step. Comparisons between different methods (to assess simulation physical validity) can be achieved by binning instances of reaction vs. time and comparing their histogram distances to the direct Gillespie method, as previously seen[54] and in **Supplemental Figure S2**.

The reaction propensity is modeled as a first order, irreversible process, as a function of a rate constant and the analyte number concentration (C_a), shown in **Equation 4**.

$$-\square_{\square} = \square_{\square} = \square_{\square\square\square}\square_{\square} = \square_{\square\square\square}\square_{\square\square\square}\square_{\square} \quad (4)$$

The rate constant k_{eff} is made to be a lumped parameter that takes into account both reactor kinetics and TAPS transport properties. Tracker microparticles are given individual treatment, randomly assigning which particle reacts when a binding event occurs. The data used for analysis is simply the excursion time until reaction (shut off) for a particle. This is retrieved from an example real system by reading which array point in the 1-D memristive array has fractionally unaltered memristance, typically defined as being 50% the conductance of a fully conductive (corresponding to the ON state) memristive channel[39]. An example of this is also included in **Supplemental S6**, although our TAPS simulation does not rely on memristor circuit modeling. We note that, due to computational constraints, the number of analyte and sensors possible to simulate simultaneously was limited, as larger C_a values make the runtime of the efficient tau-leaping method very slow or

Author Manuscript

not compilable, thus true molar (10^{23}) number concentrations could not be simulated with our scheme. The dynamics of the system would not change at these higher C_a values, only the scale of the appropriate k_{eff} values needed to map the system (this will make more sense in the context of the results).

Data Generation & Analysis

The workflow outlined in **Supplemental Figure S1c** shows how the data is processed into predicted concentration profiles in the simulation. Binned TAPS data is numerically differentiated to yield measured "reaction" rates, which is then used to solve a simultaneous, nonlinear system of elementary rate equations via the least squares method (lsqnonlin; local optimization). Initial C_a guesses are randomly varied around a fixed value (100,000) to promote finding multiple minimums. The tracker excursion times are divided into n bins (n = 30 herein, unless otherwise specified) and lumped into N sections. The number of sections is informed by prior insights on the target system; for example, there are 9 chambers of the digestive tract past the stomach. The solver uses n equations with n unknowns (n concentration variables). Each bin (n_i) inside section number (N_i) is simultaneously fitted and averaged to give a single value for each section N_i. Each fitting equation in section N_i constrains the others, as they all must satisfy the same equality within some tolerance. Unbiased upper and lower bounds (**Supplemental S3**) constrain the variables to give a realistic prediction and reduce computation time. The TAPS chemiresistors can be pre-calibrated using bench-scale experiments with similar transport properties to the system of interest, such that the effective rate constant k_{eff} for each analyte is known. As with any empirical fitting, repetitions and slight variations in model system kinetics can be used to develop a "dynamic range" of the specific chemiresistor material and the analyte of interest. In simulations, we change k_{eff} freely to evaluate its response; however, researchers employing this sensing scheme are typically limited

Author Manuscript

by the available chemical sensors, and thus a limited k_{eff} search space. These simulated experiments can inform what magnitude of analyte the distributed sensors of a specific material can accurately measure, in the context of a specific kinetic regime.

$$\square\square\square\square = \sqrt{\frac{\sum_{\square=1}^{\square} (\square_{\square} - \widehat{\square}_{\square})^2}{\square}} \quad (5)$$

Accuracy in this study is reported as a root mean square error (RMSE) evaluation (**Equation 5**), with the fitting model output (x_i) compared to the KMC simulation input ($\widehat{\square}_i$) as ground truth. For simplicity, the RMSE values have been normalized from 0 (ground truth) to 1 (null result). A null result indicates the minimum RMSE output our fitting scheme will generate when a null vector of zeros is used as a fitting input, over multiple iterations with randomized initial guesses. This RMSE value acts as a bounding cap for analysis, as any values equal to or greater than this null result are indistinguishable from nominal solver outputs. Our RMSE formula is functionally identical to performing histogram distance calculations, as mentioned above.

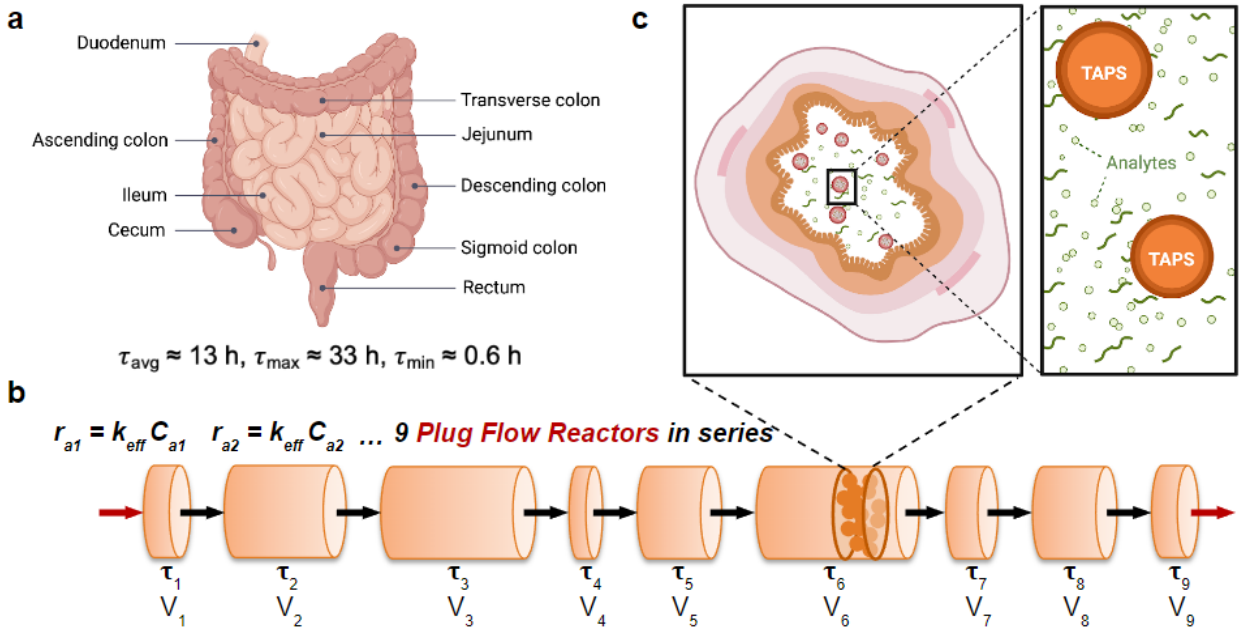
Thus far, we have discussed how k_{eff} and sensor number are key parameters in predicting TAPS effectiveness. The number of sensors is only relevant when contextualized in the scale of the analyte; thus, the sensor-normalized analyte magnitude (the ratio of analyte to TAPS sensor number, denoted herein as $\square$, where $\square = C_a/C_{TAPS}$) is utilized for analysis. Additionally, the residence time (τ) plays an important role in any reactor analysis. Kinetics determines how much system space can be sampled, but how long the sensors are given to explore that space is critical. Therefore, this study focuses on these three key parameters: k_{eff}, $\square$, τ.

Model System

Our example of an inaccessible system is poorly understood in practice and needs advanced sensing technology to measure analyte profiles: the human digestive tract. The gastrointestinal

Author Manuscript

(GI) tract, past the stomach, can be broken into 9 sections[55] (**Figure 1a**). Without loss of generality, the sample concentration profile we use is the acetic acid profile collected from cadaver sources[55]. Concentration profiles are treated as constant (unless otherwise stated) inside a single chamber, with each chamber having its respective value. Residence times for each chamber are estimated by mapping the overall excursion time to different intestine chambers by their respective volumes[56]. The general scale of τ values are shown in **Figure 1a**, with specific values provided in **Supplemental S3**. The lower GI tract is modeled here as a series of tubular plug flow reactors (PFRs), and the assumed plug flow can be rationalized if peristaltic motion has the same frequency in the radial 2-D plane, perpendicular to the axial direction of motion (**Figure 1b**)[57]. An ideal PFR residence time, modeled by a delta function, is used unless specified otherwise. Since the modeling employs plug flow, the sensors are treated as though they are stuck in a fixed (arbitrary) volume fluid element (**Figure 1c**) with a Lagrangian frame of reference and no Taylor dispersion[58], which satisfies the Gillespie algorithms need for a constant volume.



Author Manuscript

Figure 1. (a) Human intestine components and residence times (τ_i) can be represented as plug flow reactors (PFRs) **(b)**, where the time-aware particulate sensors (TAPS) are trapped in a plug flow with an equal radial distribution and an ideal (delta function) residence time distribution (RTD) **(c)**.

Results

The effect of material sensitivity (k_{eff}) *and analyte-to-sensor ratio* (□) *on TAPS profiling accuracy*

The performance of the simulated time-aware particulate sensors (TAPS) can be tuned by several key engineering parameters, one of which is the lumped effective rate constant k_{eff} that sets the sensitivity of the on-board chemiresistive sensor module (**Figure 2**). As an example, we present two simulated sensor responses (for two different k_{eff}'s) from 20,000 TAPS going through a 9-segment plug flow reactor (PFR) system. This system models a human lower GI tract with relative profiles mimicking acetic acid (analyte) concentrations in each segment[55], as well as the fitted analyte number concentrations (C_a) using the TAPS responses (**Figure 2a** and **2b**). The k_{eff} value determines how many sensors respond, and the binned profile used for fitting. High k_{eff} values, which indicate hyper-sensitivity or fast sampling, results in an erroneous number concentration fit (**Figure 2a**), whereas a five fold decrease in k_{eff} improves overall reading accuracy substantially (**Figure 2b**). In general, increased analyte sensitivity does not translate to better mapping outcomes across the board (**Figure 2c**). The error hits a minimum, the depth of which depends on how many TAPS are released. As k_{eff} increases past an optimum, the error climbs again. This behavior is due to higher sensitivities causing a higher conversion, meaning greater percentage of TAPS shut off (**Figure 2a**). As the TAPS progress down the excursion path, more unreacted sensors are depleted (**Figure 2d).** This conversion follows a sigmoidal conversion shape, in line with first order kinetics, and the confidence interval of the measurement is expected to widen; however, as the conversion of the TAPS approaches unity, the fitting algorithm receives consistently low-quality

Author Manuscript

fitting information and the error correspondingly increases to a plateau with decreased standard deviation (hence the null result; **Figure 2c**). One would expect that as more sensors are released for a given analyte number concentration (decreasing □), the climb in error due to high k_{eff} could be mitigated or delayed. This is true for a large range of □ values with diminishing returns: we observed no appreciable further decrease in fitting error for □ less than 0.003 (**Figure 2c**). These results indicate that our given system experiences accuracy saturation, despite increasing the number of TAPS deployed.

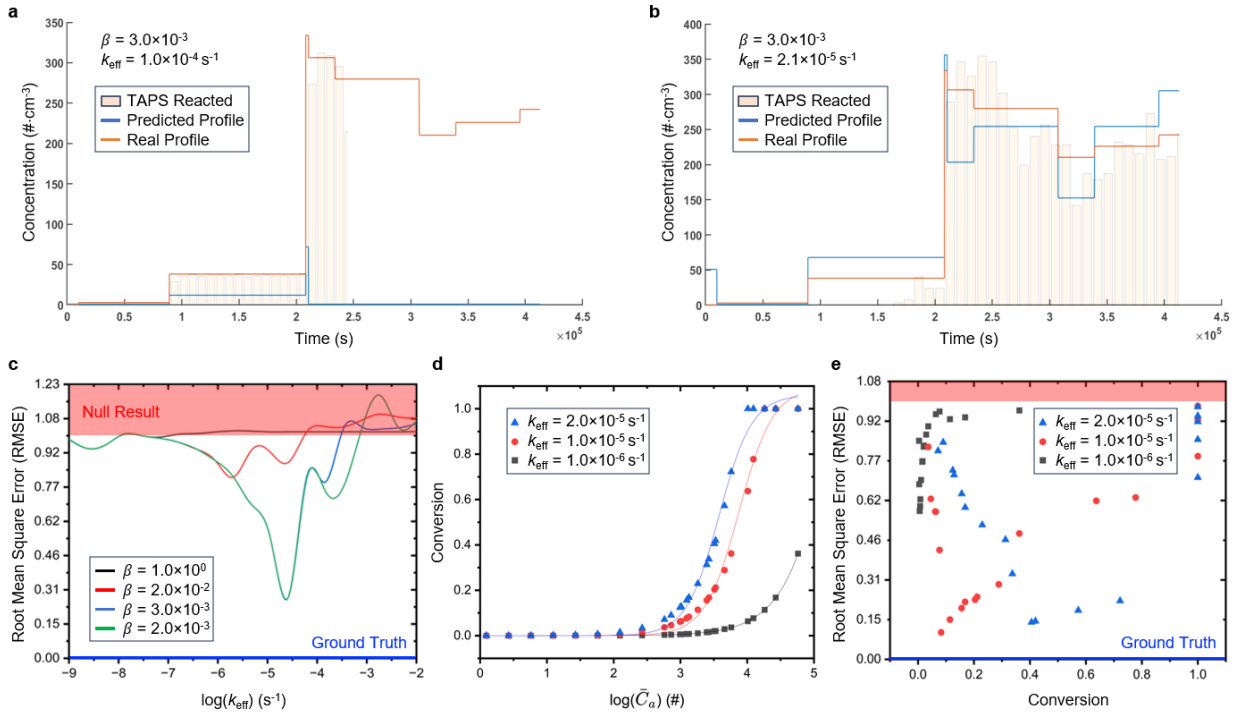


Figure 2. **(a)** For an effective rate constant (k_{eff}) value of 1.0×10^{-4} (s^{-1}) between TAPS and the acetic acid analyte, the raw binned data of TAPS reacted over time is overlaid on the actual (orange) and fitted (blue) number concentration profile for the simulated GI tract system. The analyte number concentrations in each reactor volume are kept constant. These TAPS were consumed too quickly and are unable to map the latter half of the system. **(b)** For a more appropriate k_{eff} value of 2.1×10^{-5} (s^{-1}), the TAPS system shows improved fitting performance. These TAPS last the entire excursion with enough numbers to achieve a good signal to noise ratio. **(c)** Root mean square error (RMSE) plotted as a function of k_{eff} on a base-10 logarithmic scale (log) over multiple analyte magnitudes (□) shows an optimum k_{eff} value with minimum error. As the k_{eff} increases above the optimum, the error rises again due to high consumption of TAPS. **(d)** Conversion of 50,000 released TAPS as a log function of mean analyte number concentration (C_a) is plotted at different k_{eff} values. **(e)** RMSE plotted against conversion of 50,000 released TAPS for different k_{eff} values. Regions above an RMSE value of one represent null fitting results, and an RMSE of zero denotes the ground truth.

It is worth noting the scale of the □ values and that meaningful readings take place with □ values below 1, which means there are more sensors than analyte inside the control volume. This

Author Manuscript

Author Manuscript

may seem unreasonable for practical applications, but in the context of the simulation it makes sense. The sensors are confined to a small plug volume and can only react with analyte as it enters that space. If one were to integrate the number of analytes the sensors encountered over their entire excursion in the GI tract, it can be much larger than the deployed number of sensors. In addition, this low □ result indicates these sensors would also serve well in analytical systems, where very low amounts of analyte are expected and many sensors are needed to map out a reactor volume.

Further, if conversion vs. error in **Figure 2e** is analyzed for different k_{eff} values, distinct behaviors emerge. For an "optimal" k_{eff} value (**Figure 2e**, blue), error will decrease with conversion, reach a minimum, then increase as conversion approaches unity. Below the optimum k_{eff} value (**Figure 2e**, black, red), the sensors demonstrate a similar increase in accuracy as conversion increases, but the width of the peak is narrower and the error increases more quickly. This result suggests that, when deployed as a group, the spectrum of conversion values associated with the TAPS' ability to generate reliable concentration readings widens as their analyte sensitivity is optimized. This finding also supports the idea that the collective concentration mapping capability of these computationally distributed TAPS is sensitive to their dynamics as a group within a given reactor system, particularly if they are not tuned to the k_{eff} optimum. Shifting the k_{eff} value not only changes how accurate and stable the TAPS concentration fitting can be, it also shifts the conversion value of the RMSE minimum. This result is rationalized by how more TAPS will react randomly at higher k_{eff} values, which increases the noise floor of the binned, raw data. To improve the signal to noise ratio, more TAPS must be consumed to compensate for the higher noise floor (compared to low k_{eff} systems). Thus the physical material properties of the chemi-memristive circuit elements will greatly influence what systems TAPS are useful in, but accuracy depends on more than just analyte number concentration and sensitivity.

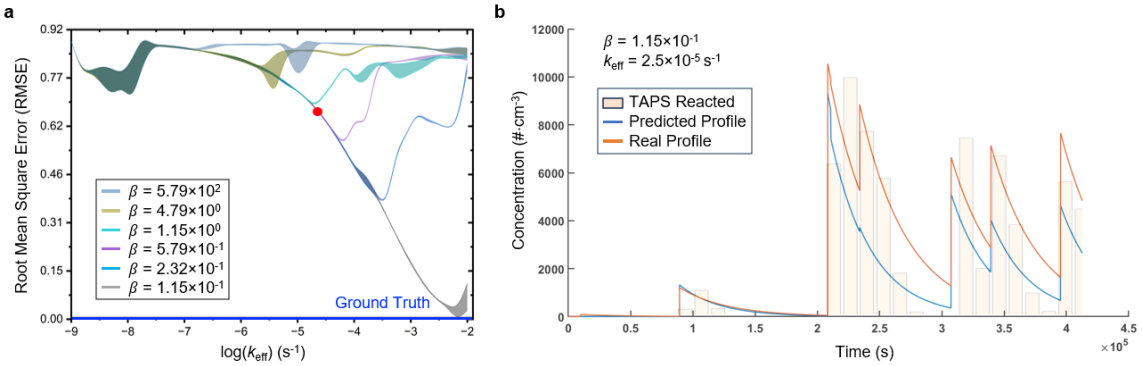


Figure 3. (a) RMSE plotted as a function of k_{eff} on a log scale over multiple □ values, for cases where analyte number concentrations in the reactor volumes are reacting with TAPS and no longer kept constant. No error saturation is seen at low □ values (more TAPS than analyte), which is improved over the constant analyte result. An RMSE of zero denotes the ground truth. **(b)** For a k_{eff} value of 2.5×10^{-4} (s^{-1}) and □ value of 0.115 (corresponding to the red point highlighted in **(a)**), the raw binned data is overlaid on the actual (orange) and fitted (blue) number concentration profile for the simulated GI tract system, which shows good fitting performance far from the minimum RMSE.

To demonstrate that these distributed TAPS can map out dynamic number concentration profiles, we simulated a modified version of the 9-PFR intestine model where the sensor/analyte interaction will result in decreases in the analyte abundance (**Figure 3**). The trends of fitting error (RMSE) plotted against the effective rate constants look similar to previous results at low k_{eff} values, where the sensor reaction kinetics are inadequate to generate a meaningful fitted analyte number concentration profile. The resulting accuracy is universally low, regardless of the number of TAPS deployed (**Figure 3a**). As k_{eff} increases, again we observe a reduction in error until the number of sensors is insufficient to accommodate the increased sensor reactivity; however, we now see a thresholding effect where increasing the number of sensors gives ideal outcomes without accuracy saturation. This makes sense due to the decreasing analyte abundance, with a proportional decrease in the probability of analyte/sensor interactions. The Poisson variable in the tau-leaping GKMC will have a shrinking distribution size and thus variance away from the mean decreases proportionally (see the **Methods** section). An example fit from such a dynamic system, shown in **Figure 3b**, demonstrates how k_{eff} values far from the optimum still have reasonable performance. The slope of the predicted and real number concentration profiles differs slightly because the

Author Manuscript

Author Manuscript

predicted lines use a fitted k_{eff} value, but the trends match well and fitted k_{eff} values are typically in the same order of magnitude as the simulation input (ground truth).

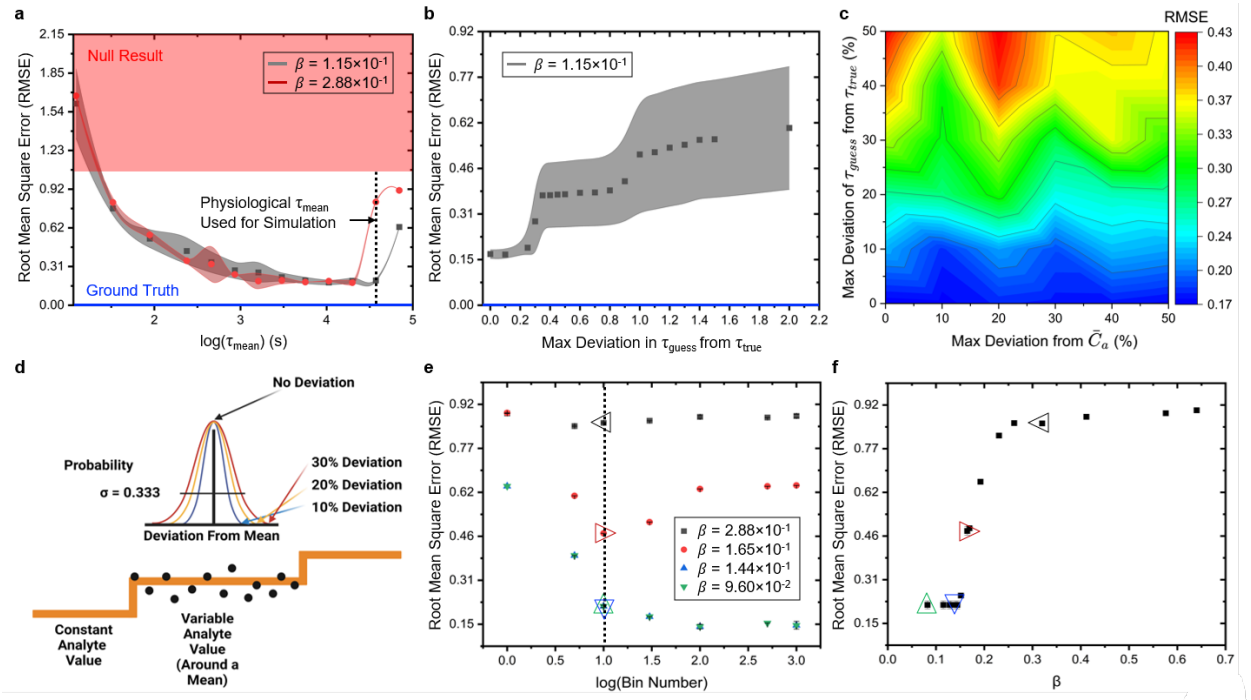
The effect of residence times* (τ) *and other simulation inputs on TAPS profiling accuracy

Residence times (τ) for computationally distributed TAPS are, in effect, the sampling time for the sensors to establish a reading. For a system with infinitely many sensors, one could argue that allowing optimized sensors to react with a fixed number concentration of analyte indefinitely will improve the confidence interval for a concentration reading. However, real systems are limited in sensor number, and care must be taken to temper their sensitivity, bundled in k_{eff}, in order to not exhaust all the TAPS at once. In fact, this parameter should be tuned not just for analyte number concentration, but also for how long it is expected to interact at that concentration. This coupling between parameters is well understood by using the Damköhler (Da) number as a metric to predict reactant conversion[1,2]. The first order Damköhler number (Da_1) is simply the kinetic constant k multiplied by the residence time τ. While our results are modeled as a first order phenomena, the results above indicate a second order relationship is more appropriate ($Da_2 = kC_a \tau$) due to higher conversion at higher C_a. The Damköhler number is derived by taking the ratio of the rate of reaction inside a control volume (V) over the analyte flux (F_a) through that volume ($\square\square = \frac{-\square_{\square}\square}{\square_{\square}}$)[1]. In our case, the TAPS are trapped in a control volume that moves through the GI tract as a plug flow with linear flow speed v_0, so $\square_{\square} = \square_{\square}\square_{\square\square\square\square}$. This results in a modified Damköhler number (Da_m) for our system, where $\square\square_{\square} = \square_{\square\square\square}\frac{\square_{\square}}{\square_{\square\square\square\square}}\square = \square_{\square\square\square}\square\square$ [=] $\frac{1}{\square}\frac{\#}{\#}\square$ [=] *1*. This derivation makes sense, as the Damköhler number is meant to indicate the extent of reactant conversion, which is the number of TAPS that reacted in our case. Large Da_m indicates high conversion, and the conversion value for a fixed kinetic regime will be inversely proportional to the number of TAPS in the system.

Author Manuscript

Simulations with low □ values (at a fixed k_{eff} value) show that as the mean system residence time (τ_{mean}) increases the error decreases accordingly (**Figure 4a)**. Very short τ_{mean} limits TAPS interaction with the environment and results in poor analyte number concentration fitting. This regime is where few analytes are interacting with the sensors, and the system approaches the "infinite sensor" regime as □ approaches 0. To minimize profiling error, the ideal scenario is to have many sensors (small □) and lots of time for them to explore the space (large τ), but as □ increases to realistic values, an optimum residence time can emerge for a given k_{eff} value due to sensor exhaustion (**Figure 4a)**. Allowing too much time for measurement is seen to actually hinder a computationally distributed scheme and adds a layer of complexity to practical implementation.

Figure 4. (a) RMSE plotted as a function of the mean system residence time over two □ values. Increasing residence



time allows the TAPS (with a k_{eff} of $2.1\times10^{-5}s^{-1}$) to more accurately fit the shape of the system, but if too much time elapses the TAPS get depleted early and fitting suffers as a result. **(b)** RMSE and its standard deviation plotted at a function of error in the guessed τ_i value used for fitting, with *x*-axis values representing the scalar multiplied by the $\tau_{i,true}$ to generate a random $\tau_{i,guess}$ (see **(d)** for details). A max deviation in τ_{guess} from τ_{true} of 1 corresponds to a maximum allowed deviation of 100% from the $\tau_{i,true}$ (so the $\tau_{i,guess}$ will have a potential minimum of 0 and maximum of $2\tau_{i,true}$). The stepped behaviors in the plot indicate when errors in guessing one τ_i grow large enough to affect other reactor sections. **(c)** RMSE is plotted as a heat map over coordinates defined by maximum deviation of instantaneous C_a from mean □□ and deviations in τ_{guess} from τ_{true}. The *y*-axis is defined analogously to the *x*-axis in **(b)** but multiplied by 100 for a percentage value. Accuracy is shown to be more sensitive to guessed τ_i values than oscillations in analyte

values. **(d)** Schematic of how τ_{guess} values are chosen to deviate from τ_{true}, as well as how the instantaneous analyte number concentration value deviates from $\square_{\square}$ are calculated. A normal distribution with mean $\square = 0$, with a standard deviation $\square = 0.333$ generates a random number (+/-), which is multiplied by a percentage of the variables' mean value, and then added to the mean to generate a guessed value. **(e)** RMSE plotted as a function of bin number (the number of partitions for raw data on the number concentration of TAPS reacted as a function of time) over multiple $\square$ values. Increasing the number of bins increases temporal resolution as long as there are enough sensors to ensure a good signal to noise ratio. **(f)** RMSE plotted as a function of $\square$ at a bin number of 10. This shows a sharp stepped behavior due to the number of bins being near the critical value (9, the number of chambers in the lower GI tract).

Additionally, the scale of the individual residence times τ_i for each reactor chamber *i* is not the only value that matters for TAPS mapping performance. Our fitting approach relies on *a priori* estimates of residence time ($\tau_{i,guess}$) to partition the binned sensor data and calculate a mean analyte value inside each compartment. This scheme is sensitive to inaccuracies in the τ_{guess} values – both the fitting error (RMSE) and the confidence interval increase substantially as the error range for the τ_{guess} increases for fixed $\square$ and k_{eff} (**Figure 4b**). For these results, τ_{guess} values are calculated by generating a normally distributed random number ($\square = 0$, $\square = 0.333$), multiplying that number by the τ_{true} values and a scalar (where the *x*-axis in **Figure 4b** denotes that scalar value) which is then added to the τ_{true} values to generate τ_{guess}. A visualization is depicted similarly for analyte profiles in **Figure 4d**, and the equation is provided in **Supplemental Figure S3**. In this method, the error in chosen τ_{guess} earlier in the intestinal excursion (say chamber 2) will propagate to subsequent chambers, and thus doing multiple simulation iterations (an $n = 30$ in this case) allows a combinatorial evaluation of accuracy performance. It is worth noting that the stepping behavior seen in **Figure 4b** is not universal, but specific to the reactor system of choice and dependent on the distribution of τ_i values in the 9-PFR representation of the digestive tract (along with k_{eff} and $\square$). The stepped increase in RMSE after some threshold indicates when the τ_{guess}'s propagated error is large enough to shift the mean RMSE. While this sensitivity to inaccuracies of reactor residence times poses a significant challenge in the practical implementation of the TAPS distributed sensing scheme, obtaining accurate residence time distributions (RTD) is also a

Author Manuscript

problem chemical engineers are familiar with solving[1,2]. Inert tracers (even memristive ones) can be used to elucidate the RTD of each PFR segment, with special considerations necessary for systems with non-ideal flow profile (such as the intestine with peristalsis). Similar to that shown by De la Paz *et al.*[21], an IC pill sensor also needs to combine with x-ray imaging (or other tracking methods) to fully elucidate the path and duration of a plug flow element in the GI tract.

On the other hand, the profiles fitted from simulated TAPS responses exhibit high stability against number concentration swings of the analyte. To probe this, we tested how the system would respond to having analyte profile distributions fixed around a mean (**Figure 4d**). A cross comparison of deviance in τ_{guess} and analyte variance around a mean (**Figure 4c**) highlights the system's greater sensitivity to τ_{guess} rather than analyte concentration fluctuations. This result indicates that small oscillations in the actual analyte profile will not disturb readings, so long as the τ_{guess} is accurate.

Other parameters such as the temporal resolution of TAPS measurements also impact their concentration mapping capability, illustrated here using scenarios where a single, mean analyte value is used for each reaction chamber (**Figure 4e** and **4f**). In our workflow, TAPS temporal resolution can be dynamically adjusted via binning the excursion time axis. Until this point, the number of bins we lump TAPS data into has been fixed at 30 to allow for at least 3 data points in each of the 9 lower GI tract PFRs to fit the data. In reality, the number of bins is only practically limited by the measurement resolution of the fabricated TAPS memristor array, or more generally the temporal resolution for TAPS that do not rely on 1-D memristor arrays as their time-keeping mechanism[15,39]. **Figure 4e** shows the behavior of different analyte/sensor ratios (□) for a fixed k_{eff} value and $\tau_{guess} = \tau_{true}$. The bin number is defined by TAPS temporal resolution Δt and having more bins will decrease Δt, which necessitates that the precision of the measurement for when the sensor

Author Manuscript

Author Manuscript

reacts must also increase. Increasing the number of bins past 9 (the number of chambers in the lower GI tract) shows a thresholding effect, where systems with insufficient number of TAPS (higher □) lose measurement fidelity and see fitting error increases (**Figure 4e**, black and red). This can be explained by the fact that the binned information is simply a count of how many sensors detected enough analyte to "react" at a time *t*. Increasing the number of bins lowers the maximum counted values and thus brings signal data closer to background noise. As the bin number approaches the number of sensors deployed, the binned profile will look binary, where the true signal is indistinguishable from noise, and the fitting will suffer as a result. Conversely, at the lower limit of a single bin, only a single value is produced, there is no temporal or spatial resolution, and RMSE is high. As we increase the number of TAPS deployed to allow for increased binning, the profiling error can indeed be reduced below that obtained at the critical bin number of 9, but the gain in fitting quality saturates quickly (**Figure 4e**, blue and green). To highlight this saturation effect, we plot the fitting RMSE against □ at a fixed bin number of 10 (**Figure 4f**). It shows the plateauing fitting errors for □ less than 0.15. This finding further demonstrates how increasing the number of TAPS deployed (lowering □) can have diminishing returns at a fixed k_{eff} value.

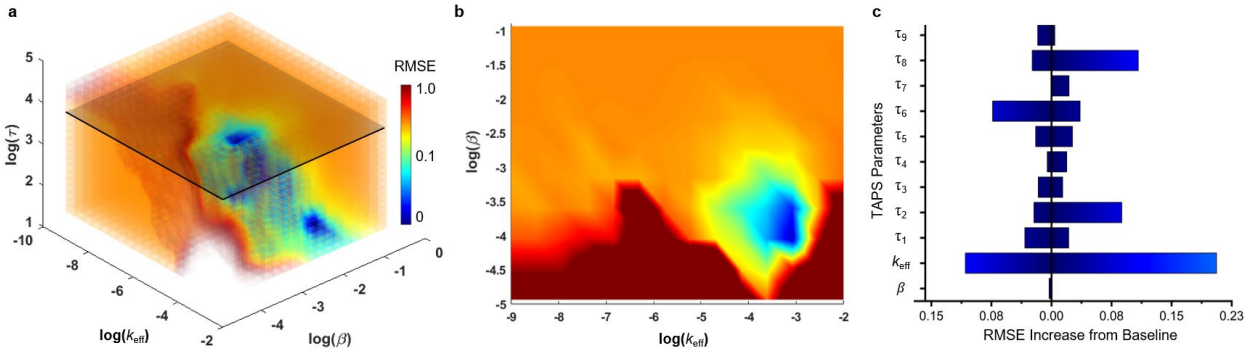


Figure 5. (a) A 3-D heatmap of RMSE plotted as a function of TAPS simulation parameters k_{eff}, □, and τ on log scales, with blue regions being close to ground truth for a given system and the kinetic regime. **(b)** The z plane 2-D cross-section corresponding to the τ values in the human lower GI tract used in previous simulations is highlighted. **(c)** A sensitivity analysis conducted at optimized TAPS deployment parameters for the human lower GI tract (log(□) = -3.7, k_{eff} = 6×10^{-4} s^{-1}, baseline RMSE = 0.05) show no substantial disturbance in the fitting accuracy if simulation

inputs are varied by +/- 20%. The residence times for each chamber were varied independently in the KMC simulation, and the fitting utilized the τ_{true} values for binning. 70,000 TAPS sensors were simulated at a log(□) = -3.7.

The results shown thus far have been parametric evaluations of the key parameters k_{eff}, □, and τ. The plots presented are in fact 2-D cross sections of what is a 3-D search space, with the dimensions defined by the above variables. For a given system it is advisable to plot the accuracy across all 3 dimensions to globally identify regions of material sensitivity and analyte scale that would generate meaningful concentration profiling results. **Figure 5a** visualizes the 3-D search space of the idealized 9-PFR lower GI tract system, with blue regions being closer to ground truth and color values above 1 (null result) have been made transparent. Inside the KMC simulation, k_{eff} values were allowed to deviate from their input value by up to 20% of the input value (the scheme in **Figure 4d**), which helps identify regions of stability and is more representative of a real system where the k_{eff} may fluctuate over time. Representative □ and τ values are calculated simply by taking the mean values for all sections of the 9-PFR system. We can clearly see a blue vein running through the 3-D parameter space, which shows low RMSE results. In our case, the τ depends on the specific reactor system where TAPS are deployed and is typically not a controllable engineering parameter. Practically, the k_{eff} and □ for TAPS must be tuned to high accuracy regions for any specific reactor system with a given τ. For example, the circulatory system is characterized by residence times much less than those of the digestive tract, and engineers can use these types of 3-D fitting quality maps to quickly identify relevant sensor parameters for various analytes of interest. Additionally, if we were to shuffle the order of the reactor tanks in the intestine system presented here, a new optimum k_{Eff} would need to be identified (**Supplemental Figure 7**). Again, TAPS are not tied to a particular sensing-recording technology, such as 1-D memristor arrays. We present TAPS as a moniker for a system optimization scheme of handling colloidal-scale, computationally limited sensors, as long as they possess the ability to timestamp a single analyte

Author Manuscript

detection event. Thus any technology that fits into this category can benefit from this analysis, regardless of the target system.

Even within the lower GI tract system, different individuals tend to have different mean residence times, which adds value to this comprehensive 3D variable visualization. At low mean τ values, higher TAPS sensitivity (k_{eff}) are needed to quickly respond to analytes due to the limited sampling time. As the mean τ increases, the high accuracy region shifts towards lower k_{eff} and □ values; as TAPS are given more time to interact with the analyte, they do not need to be as sensitive and more sensors are needed to maintain an adequate signal to noise ratio.

As an example, we show the 2-D *z*-slice of the τ values relevant to the human GI tract values used herein (**Figure 5b)**, and the blue region can easily be identified to choose a range of k_{eff} and □ values. Lower □ values than those shown in **Figures 2** and **Figure 3** depict the highest accuracy region actually being closer to k_{eff} values of 1×10^{-3} (s^{-1}) than 1×10^{-5} (s^{-1}). Further, when pushing to even lower □ values, we see that hyper-analytical systems (orders of magnitude less analyte than sensors) do not produce good fitting results across all k_{eff} values screened in this study. A sensitivity analysis around the optimized process parameters in **Figure 5b** (where □ = $2.\times10^{-4}$ and $k_{eff} = 6.0\times10^{-4}$ s^{-1} with a baseline RMSE of 0.05) indicates that, for this 9-PFR system, varying system parameters by ±20% does not substantially disrupt TAPS profiling accuracy (**Figure 5c**). As expected, the most sensitive parameter is the k_{eff} value. Taken together, these results indicate that optimized sensors should display reproducible performance in spite of noise and reasonable fluctuations in process parameters.

Discussion

Through the simulated deployment of computationally distributed time-aware particulate sensor (TAPS) networks, we have established a framework for their practical implementation to

Author Manuscript

Author Manuscript

profile analyte concentrations in systems of chemical reactors. This builds on the previously reported timing mechanism concept in a one-dimensional (1-D) memristor array. However, the aspects of computationally distributed sensors discussed herein apply beyond the memristive framework. Any current or future tracer technologies that can locally encode analyte detection times qualify as TAPS and can easily be integrated into the framework presented in this study. We demonstrate that TAPS can be used to accurately map concentration profiles, such as the acetic acid levels in human lower GI tract, with a large dynamic range in analyte number concentration magnitude and sensor residence times. More generally, we show that the sensor material properties must not only be tuned for analyte concentrations but also expected residence times. Calculations of the modified Damköhler number (Da_m) for the system averaged values show good agreement with overall conversion numbers (**Supplemental Figure S4)**, and indicate that systems with Da_m values above 0.01 are expected to have at least 80% conversion. Our analysis highlights the importance of *a priori* system knowledge on residence times of the corresponding reactor system, which can be obtained via existing inert tracer methods[1,2,39].

The 1-D memristor arrays, used here as an example, are not the "final form" of microscale analog computation schemes. Previous work has shown that memristor circuits can act as microscale "point" sensors by implementing many 1-D arrays in parallel (a 2-D array). In that scheme, a main 1-D memristive array (or trunk) is connected directly to the voltage source, with many 1-D arrays branching off. The trunk has fixed resistors, and thus a switching time insensitive to the chemical environment. The chemically sensitive material coats only the branch arrays and permits simultaneous objective timekeeping[39]. However, 2-D memristor arrays are more complicated to fabricate and currently unrealizable at a colloidal scale[15,29,39]. Until better fabrication methods arise, the computationally-limited, distributed TAPS scheme presented in this

work remains a more realistic alternative with broad applicability. Previous efforts have identified effects of fabrication variability on single sensor TAPS-type readings[39] and we extend these results in **Supplementary S7** using distributions of k_{Eff} values to probe ensemble TAPS readings.

The results presented herein can also be extended to systems where sensors have anisotropic position distributions or dispersion of residence times, and the well mixed condition is not met, by using refined meshed domains combined with Gillespie KMC. In this study, we demonstrate the tau-leaping Gillespie Kinetic Monte Carlo implementation for simple model systems where fluid dynamics are well characterized. Extra care needs to be taken for the analysis and concentration profiling of the real GI tract, where the fluid dynamics are peristaltic in nature, and variable depending on individual feeding cycles. Furthermore, dispersion of residence times in these sensors can be practically accounted for by having a 1-D memristive array without chemically sensitive components next to the chemically sensitive array. This would ensure one array can keep track of time passing and one array could sense the time it detected analyte.

Another factor not heavily considered here is the effect of the nonlinear fitting hyperparameters on system performance. Choosing boundary conditions, initial guesses, and solver tolerances will affect the accuracy in a real-life system. This would involve tailoring the analysis scheme to the system of interest and ensuring that the parameters are loose enough to explore the global optimization space while also being precise enough to prevent the solver settling into an inadequate minimum. For the purpose of this investigation, we manually identified solver settings that could generate a distribution of reproducible results, while trying to avoid overfitting certain data. Our intention was not to contrive a system with "100% accuracy", and thus the accuracy/RMSE values reported should not imply absolute limits on system performance.

Data Availability and Reproducibility Statement

Author Manuscript

Author Manuscript

The data that supports the findings of this study are available in the supplementary material of this article. There are additionally some data and example code files, with notes on inputs and considerations in the **Supplemental S3** & **S5**. **Supplemental S2** contains model validation that our code, at a basic level, can mimic programmable chemical reactions, and we evaluate our use of the approximate Gillespie method vs the Direct (true) method and find little drop off in accuracy. **Supplemental S3** contains inputs and specifications for our nonlinear optimization function, with notes.

Conclusions

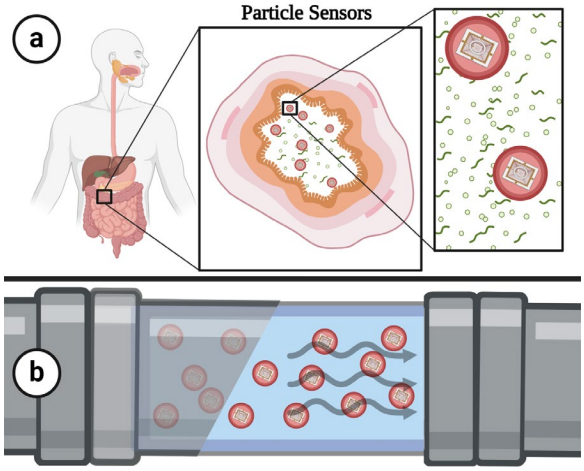
In summary, computationally limited, time-aware particulate sensing (TAPS) platforms show great potential to map analyte distributions at the microscale, when used as an ensemble. The analyte concentration profiling performance of the collective of sensor nodes is heavily dependent on the sensitivity and sampling environment (k_{eff}) of the chemical sensor used to detect the analyte, as well as the sampling time (τ) and analyte to sensor ratio (□). We have outlined a process to simulate TAPS in any system with considerations for how to progress such a scheme from experiments *in silico* to *in vitro*. We see the near future of this technology as reliant on the development of materials with non-volatile memory properties and microscale energy autonomy; however, advances in IC-based control systems should not be ruled out long term, and considerations herein can be extended to any simplistic microsensor technology so long as they are time-aware.

Plain Language Summary

We show that if simple sensors can remember both the passage of time and the time when they encounter a chemical stimulus, they collectively can map concentration profiles in complex reactor systems when deployed in large quantities.

Author Manuscript

Graphical Abstract



Author Manuscript

References

1. Fogler HS. *Elements of Chemical Reaction Engineering*. Pearson Educación; 1999.
2. Levenspiel O. *Chemical Reaction Engineering*. John Wiley & Sons; 1998.
3. Thorsen T, Maerkl SJ, Quake SR. Microfluidic Large-Scale Integration. *Science*. 2002;298(5593):580-584. doi:10.1126/science.1076996
4. Wang S, Lin JR, Sontag ED, Sorger PK. Inferring reaction network structure from single-cell, multiplex data, using toric systems theory. *PLOS Computational Biology*. 2019;15(12):e1007311. doi:10.1371/journal.pcbi.1007311
5. Engblom S, Wilson DB, Baker RE. Scalable population-level modelling of biological cells incorporating mechanics and kinetics in continuous time. *Royal Society Open Science*. 2018;5(8):180379. doi:10.1098/rsos.180379
6. Conlon MJ, Russell DL, Mussivand T. Development of a Mathematical Model of the Human Circulatory System. *Ann Biomed Eng*. 2006;34(9):1400-1413. doi:10.1007/s10439-006-9164-y
7. Transport of reactive contaminants in heterogeneous porous media - Brusseau - 1994 - Reviews of Geophysics - Wiley Online Library. Accessed May 1, 2024. https://agupubs.onlinelibrary.wiley.com/doi/10.1029/94RG00624
8. Prud'Homme R. Chemical Reactors. In: *Flows and Chemical Reactions in Homogeneous Mixtures*. John Wiley & Sons, Ltd; 2013:47-78. doi:10.1002/9781118832653.ch2
9. Ptak T, Piepenbrink M, Martac E. Tracer tests for the investigation of heterogeneous porous media and stochastic modelling of flow and transport—a review of some recent developments. *Journal of Hydrology*. 2004;294(1):122-163. doi:10.1016/j.jhydrol.2004.01.020
10. Mamas M, Dunn WB, Neyses L, Goodacre R. The role of metabolites and metabolomics in clinically applicable biomarkers of disease. *Arch Toxicol*. 2011;85(1):5-17. doi:10.1007/s00204-010-0609-6
11. Broza YY, Zhou X, Yuan M, et al. Disease Detection with Molecular Biomarkers: From Chemistry of Body Fluids to Nature-Inspired Chemical Sensors. *Chem Rev*. 2019;119(22):11761-11817. doi:10.1021/acs.chemrev.9b00437
12. Bakh NA, Bisker G, Lee MA, Gong X, Strano MS. Rational Design of Glucose-Responsive Insulin Using Pharmacokinetic Modeling. *Advanced Healthcare Materials*. 2017;6(22):1700601. doi:10.1002/adhm.201700601
13. Lee MA, Bakh N, Bisker G, Brown EN, Strano MS. A Pharmacokinetic Model of a Tissue Implantable Cortisol Sensor. *Advanced Healthcare Materials*. 2016;5(23):3004-3015. doi:10.1002/adhm.201600650
14. Bisker G, Iverson NM, Ahn J, Strano MS. A Pharmacokinetic Model of a Tissue Implantable Insulin Sensor. *Advanced Healthcare Materials*. 2015;4(1):87-97. doi:10.1002/adhm.201400264
15. Zhang G, Yang JF, Yang S, et al. Colloidal State Machines as Smart Tracers for Chemical Reactor Analysis. *Advanced Intelligent Systems*. n/a(n/a):2300130. doi:10.1002/aisy.202300130
16. Tenney RR, Sandell NR. Detection with Distributed Sensors. *IEEE Transactions on Aerospace and Electronic Systems*. 1981;AES-17(4):501-510. doi:10.1109/TAES.1981.309178
17. Eschenauer L, Gligor VD. A key-management scheme for distributed sensor networks. In: *Proceedings of the 9th ACM Conference on Computer and Communications Security*. CCS '02. Association for Computing Machinery; 2002:41-47. doi:10.1145/586110.586117
18. Wireless Sensor Networks for Distributed Chemical Sensing: Addressing Power Consumption Limits With On-Board Intelligence | IEEE Journals & Magazine | IEEE Xplore. Accessed October 2, 2023. https://ieeexplore.ieee.org/abstract/document/5585658

Author Manuscript

19. Seo D, Neely RM, Shen K, et al. Wireless Recording in the Peripheral Nervous System with Ultrasonic Neural Dust. *Neuron*. 2016;91(3):529-539. doi:10.1016/j.neuron.2016.06.034
20. Carrara S. Body Dust: Well Beyond Wearable and Implantable Sensors. *IEEE Sensors Journal*. 2021;21(11):12398-12406. doi:10.1109/JSEN.2020.3029432
21. De la Paz E, Maganti NH, Trifonov A, et al. A self-powered ingestible wireless biosensing system for real-time in situ monitoring of gastrointestinal tract metabolites. *Nat Commun*. 2022;13(1):7405. doi:10.1038/s41467-022-35074-y
22. Sharma S, Ramadi KB, Poole NH, et al. Location-aware ingestible microdevices for wireless monitoring of gastrointestinal dynamics. *Nat Electron*. 2023;6(3):242-256. doi:10.1038/s41928-023-00916-0
23. Kalantar-Zadeh K, Berean KJ, Ha N, et al. A human pilot trial of ingestible electronic capsules capable of sensing different gases in the gut. *Nat Electron*. 2018;1(1):79-87. doi:10.1038/s41928-017-0004-x
24. Steiger C, Abramson A, Nadeau P, Chandrakasan AP, Langer R, Traverso G. Ingestible electronics for diagnostics and therapy. *Nat Rev Mater*. 2019;4(2):83-98. doi:10.1038/s41578-018-0070-3
25. Inda-Webb ME, Jimenez M, Liu Q, et al. Sub-1.4 cm3 capsule for detecting labile inflammatory biomarkers in situ. *Nature*. 2023;620(7973):386-392. doi:10.1038/s41586-023-06369-x
26. Cortese AJ, Smart CL, Wang T, et al. Microscopic sensors using optical wireless integrated circuits. *Proceedings of the National Academy of Sciences*. 2020;117(17):9173-9179. doi:10.1073/pnas.1919677117
27. Lee S, Cortese AJ, Gandhi AP, Agger ER, McEuen PL, Molnar AC. A 250 μm × 57 μm Microscale Opto-electronically Transduced Electrodes (MOTEs) for Neural Recording. *IEEE Trans Biomed Circuits Syst*. 2018;12(6):1256-1266. doi:10.1109/TBCAS.2018.2876069
28. Smart CL, Cortese AJ, Ramshaw BJ, McEuen PL. Nanocalorimetry using microscopic optical wireless integrated circuits. *Proceedings of the National Academy of Sciences*. 2022;119(45):e2205322119. doi:10.1073/pnas.2205322119
29. Liu AT, Hempel M, Yang JF, et al. Colloidal robotics. *Nat Mater*. Published online August 24, 2023:1-10. doi:10.1038/s41563-023-01589-y
30. Materializing Autonomy in Soft Robots across Scales - Berrueta - Advanced Intelligent Systems - Wiley Online Library. Accessed October 2, 2023. https://onlinelibrary.wiley.com/doi/full/10.1002/aisy.202300111
31. Mo Y, Lu Z, Rughoobur G, et al. Microfluidic electrochemistry for single-electron transfer redox-neutral reactions. *Science*. 2020;368(6497):1352-1357. doi:10.1126/science.aba3823
32. Köhne JM, Köhne S, Šimůnek J. A review of model applications for structured soils: a) Water flow and tracer transport. *Journal of Contaminant Hydrology*. 2009;104(1):4-35. doi:10.1016/j.jconhyd.2008.10.002
33. Koman VB, Liu P, Kozawa D, et al. Colloidal nanoelectronic state machines based on 2D materials for aerosolizable electronics. *Nat Nanotechnol*. 2018;13(9):819-827. doi:10.1038/s41565-018-0194-z
34. Reynolds MF, Cortese AJ, Liu Q, et al. Microscopic robots with onboard digital control. *Science Robotics*. 2022;7(70):eabq2296. doi:10.1126/scirobotics.abq2296
35. Molnar AC, Lee S, Cortese A, McEuen P, Sadeghi S, Ghajari S. Nanoliter-Scale Autonomous Electronics: Advances, Challenges, and Opportunities. In: *2021 IEEE Custom Integrated Circuits Conference (CICC)*. ; 2021:1-6. doi:10.1109/CICC51472.2021.9431529
36. Law J, Yu J, Tang W, Gong Z, Wang X, Sun Y. Micro/Nanorobotic Swarms: From Fundamentals to Functionalities. *ACS Nano*. 2023;17(14):12971-12999. doi:10.1021/acsnano.2c11733
37. Liu P, Liu AT, Kozawa D, et al. Autoperforation of 2D materials for generating two-terminal memristive Janus particles. *Nature Mater*. 2018;17(11):1005-1012. doi:10.1038/s41563-

018-0197-z
38. Hempel M, Schroeder V, Park C, et al. SynCells: A 60 × 60 μm2 Electronic Platform with Remote Actuation for Sensing Applications in Constrained Environments. *ACS Nano*. 2021;15(5):8803-8812. doi:10.1021/acsnano.1c01259
39. Yang JF, Liu AT, Berrueta TA, et al. Memristor Circuits for Colloidal Robotics: Temporal Access to Memory, Sensing, and Actuation. *Advanced Intelligent Systems*. 2022;4(4):2100205. doi:10.1002/aisy.202100205
40. Chen H, Wang Y, Liu Y, Zou Q, Yu J. Sensing of Fluidic Features Using Colloidal Microswarms. *ACS Nano*. 2022;16(10):16281-16291. doi:10.1021/acsnano.2c05281
41. Zhu M, Schmidt OG. Batteries for small-scale robotics. *MRS Bulletin*. 2024;49(2):115-124. doi:10.1557/s43577-023-00651-z
42. Zhang G, Yang J, Gonzalez-Medrano D, et al. High Energy Density Picoliter Zn-Air Batteries for Colloidal Robots and State Machines. Published online August 11, 2022. doi:10.26434/chemrxiv-2022-20jjz-v2
43. Guo T, Sun B, Ranjan S, et al. From Memristive Materials to Neural Networks. *ACS Appl Mater Interfaces*. 2020;12(49):54243-54265. doi:10.1021/acsami.0c10796
44. Strukov DB, Snider GS, Stewart DR, Williams RS. The missing memristor found. *Nature*. 2008;453(7191):80-83. doi:10.1038/nature06932
45. Knapp JLA, González-Pinzón R, Haggerty R. The Resazurin-Resorufin System: Insights From a Decade of “Smart” Tracer Development for Hydrologic Applications. *Water Resources Research*. 2018;54(9):6877-6889. doi:10.1029/2018WR023103
46. Bottacin-Busolin A, Dallan E, Marion A. STIR-RST: A Software tool for reactive smart tracer studies. *Environmental Modelling & Software*. 2021;135:104894. doi:10.1016/j.envsoft.2020.104894
47. Hawkins AJ, Bender JT, Grooms RD, Schissel CJ, Tester JW. Temperature-responsive smart tracers for field-measurement of inter-well thermal evolution: Heterogeneous kinetics and field demonstration. *Geothermics*. 2021;92:102046. doi:10.1016/j.geothermics.2021.102046
48. Cao V, Schaffer M, Taherdangkoo R, Licha T. Solute Reactive Tracers for Hydrogeological Applications: A Short Review and Future Prospects. *Water*. 2020;12(3):653. doi:10.3390/w12030653
49. Schaffer M, Maier F, Licha T, Sauter M. A new generation of tracers for the characterization of interfacial areas during supercritical carbon dioxide injections into deep saline aquifers: Kinetic interface-sensitive tracers (KIS tracer). *International Journal of Greenhouse Gas Control*. 2013;14:200-208. doi:10.1016/j.ijggc.2013.01.020
50. Das S, Vikalo H, Hassibi A. Stochastic modeling of reaction kinetics in biosensors using the Fokker Planck equation. In: *2009 IEEE International Workshop on Genomic Signal Processing and Statistics*. ; 2009:1-4. doi:10.1109/GENSIPS.2009.5174363
51. Hassibi A, Vikalo H, Hajimiri A. On noise processes and limits of performance in biosensors. *Journal of Applied Physics*. 2007;102(1):014909. doi:10.1063/1.2748624
52. Andersen M, Panosetti C, Reuter K. A Practical Guide to Surface Kinetic Monte Carlo Simulations. *Frontiers in Chemistry*. 2019;7. Accessed August 10, 2023. https://www.frontiersin.org/articles/10.3389/fchem.2019.00202
53. Gillespie DT. Exact stochastic simulation of coupled chemical reactions. *J Phys Chem*. 1977;81(25):2340-2361. doi:10.1021/j100540a008
54. Cao Y, Samuels DC. Discrete Stochastic Simulation Methods for Chemically Reacting Systems. *Methods Enzymol*. 2009;454:115-140. doi:10.1016/S0076-6879(08)03805-6
55. Cummings JH, Pomare EW, Branch WJ, Naylor CP, Macfarlane GT. Short chain fatty acids in human large intestine, portal, hepatic and venous blood. *Gut*. 1987;28(10):1221-1227. doi:10.1136/gut.28.10.1221
56. Stubbs DF. Models of gastric emptying. *Gut*. 1977;18(3):202-207.

Author Manuscript

57. Floryan JM, Panday S, Faisal KhMd. On the peristaltic pumping. *Physics of Fluids*. 2021;33(3):033609. doi:10.1063/5.0042883
58. Taylor GI. Diffusion by Continuous Movements. *Proceedings of the London Mathematical Society*. 1922;s2-20(1):196-212. doi:10.1112/plms/s2-20.1.196

Author Manuscript

Author Manuscript

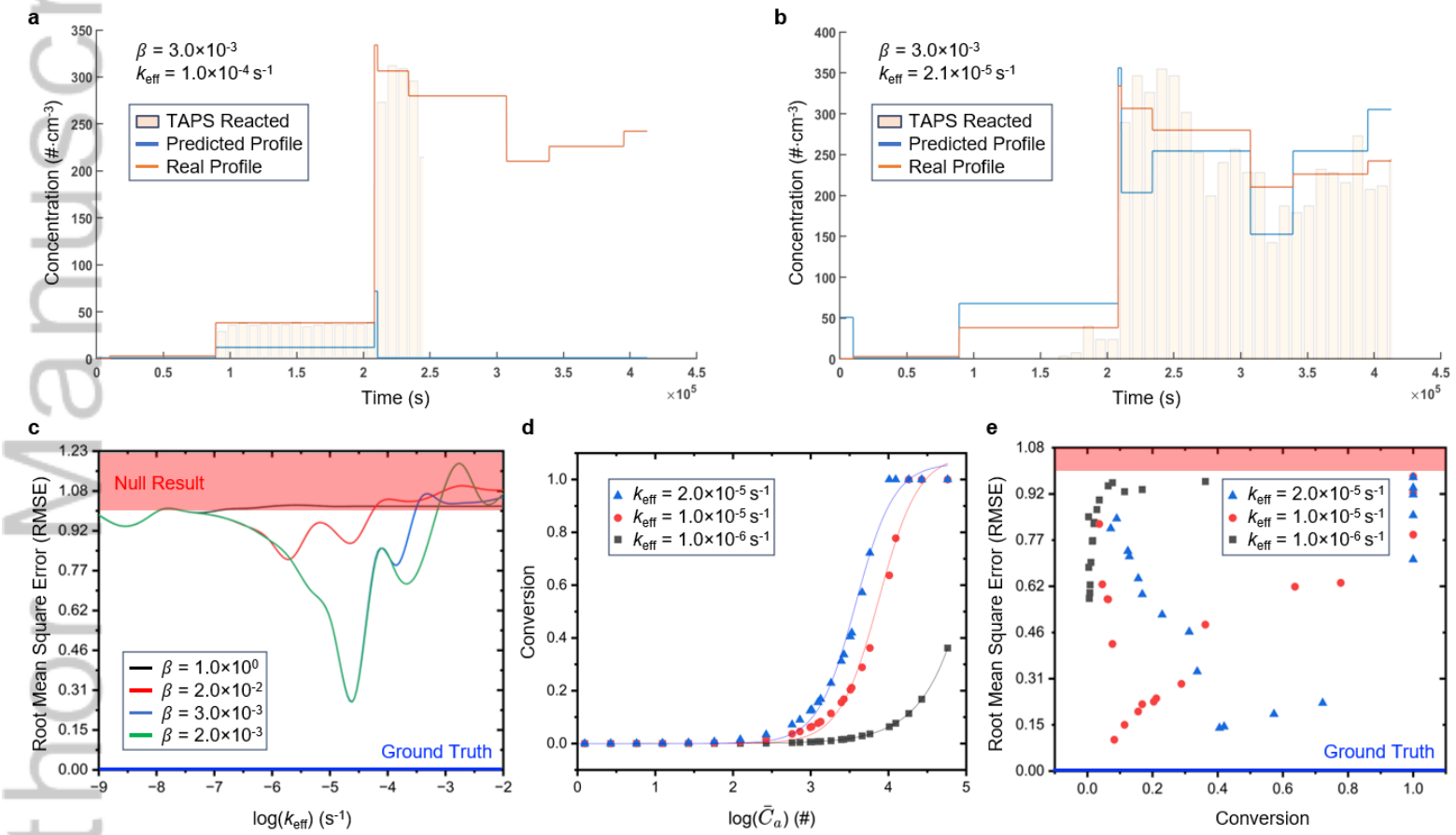


fig2_0507.tiff

Author Manuscript

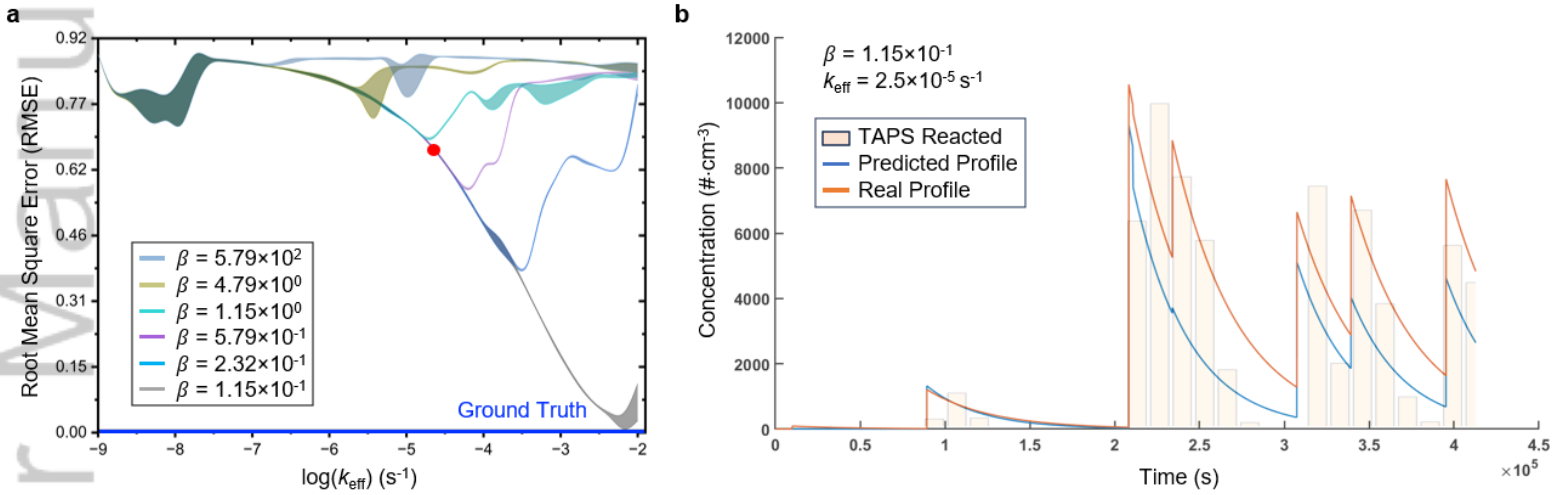


fig3_0507.tiff

Author Manuscript

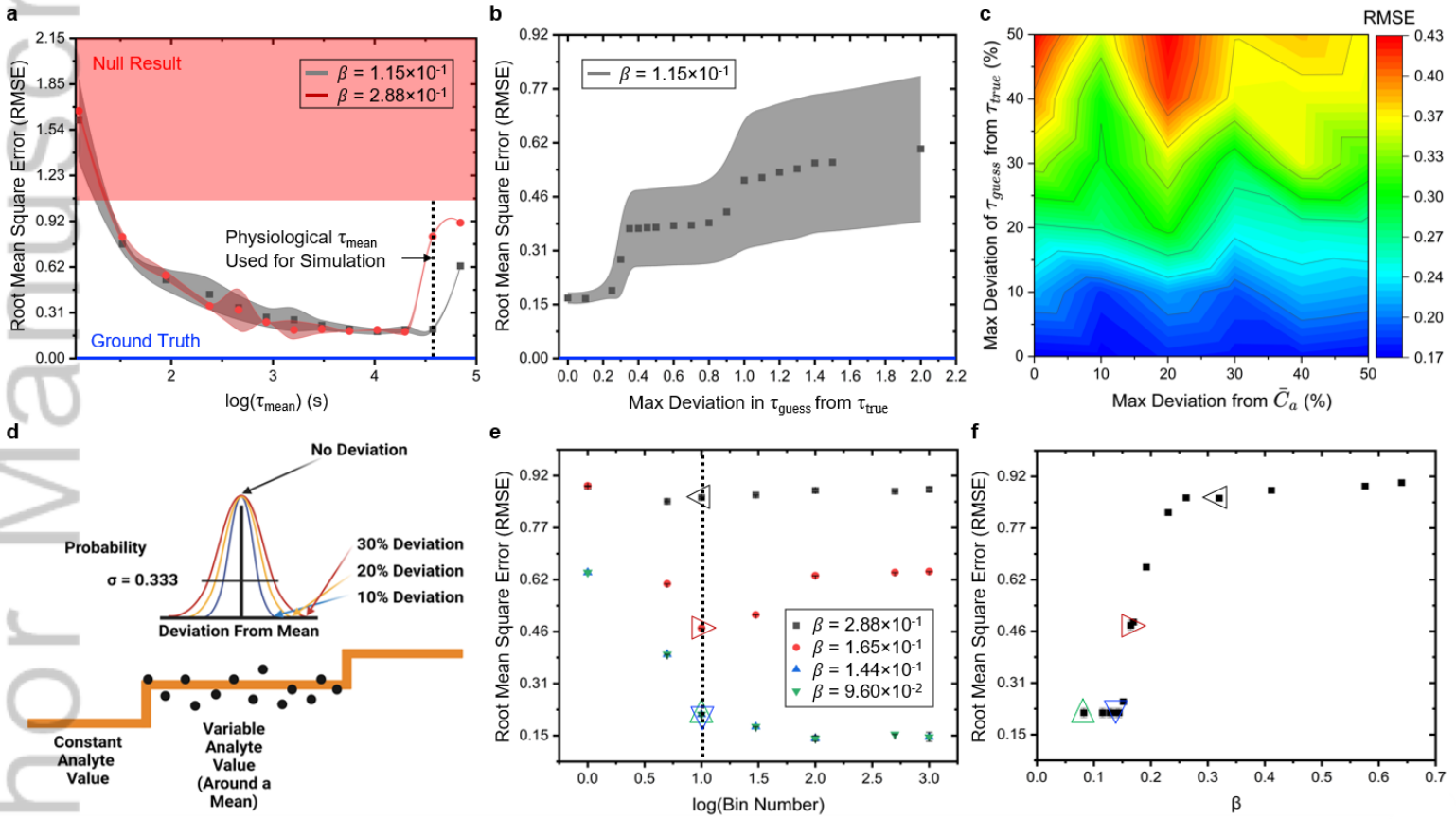


fig4_0507.tiff

Author Manuscript

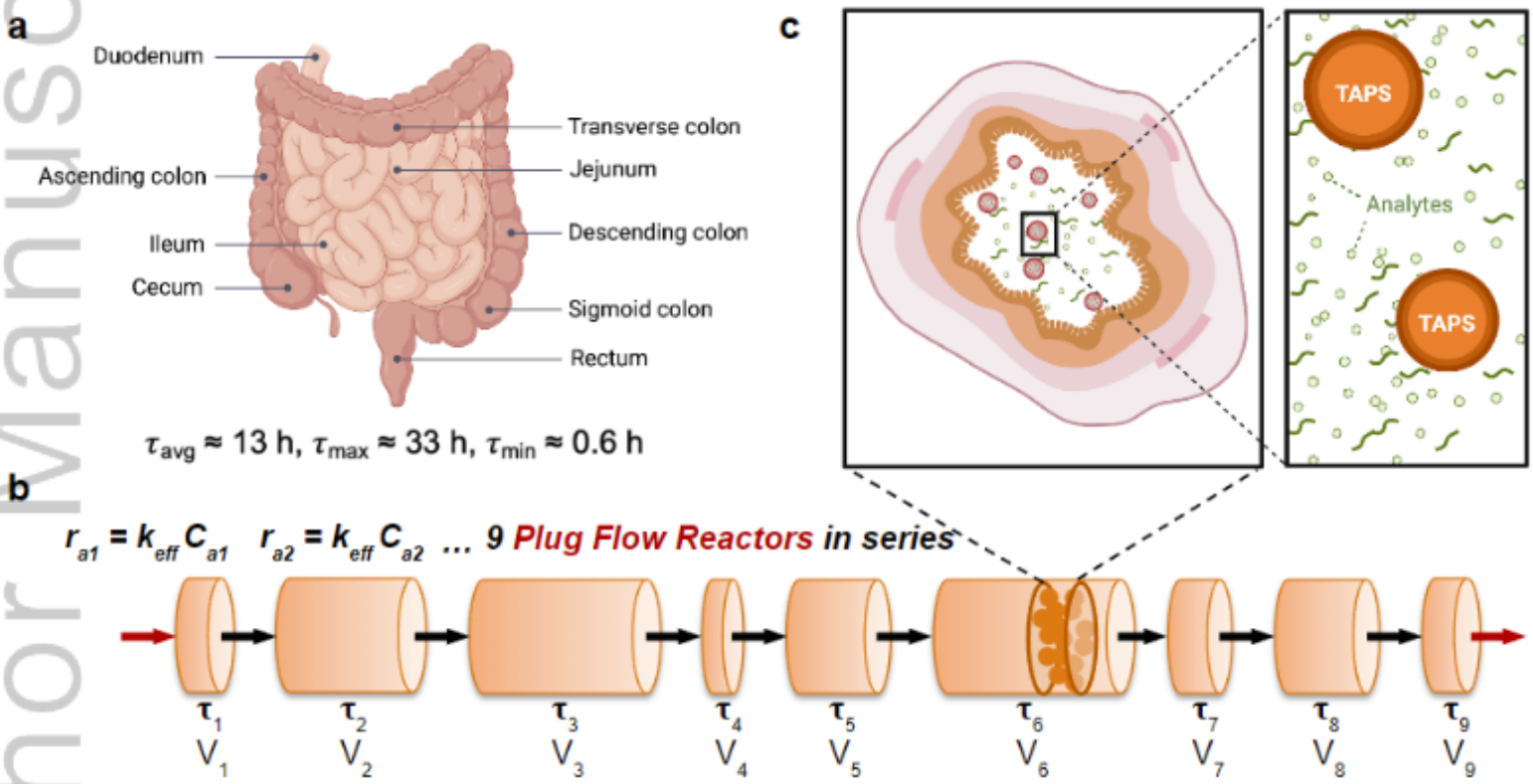


Figure1.png

Author Manuscript

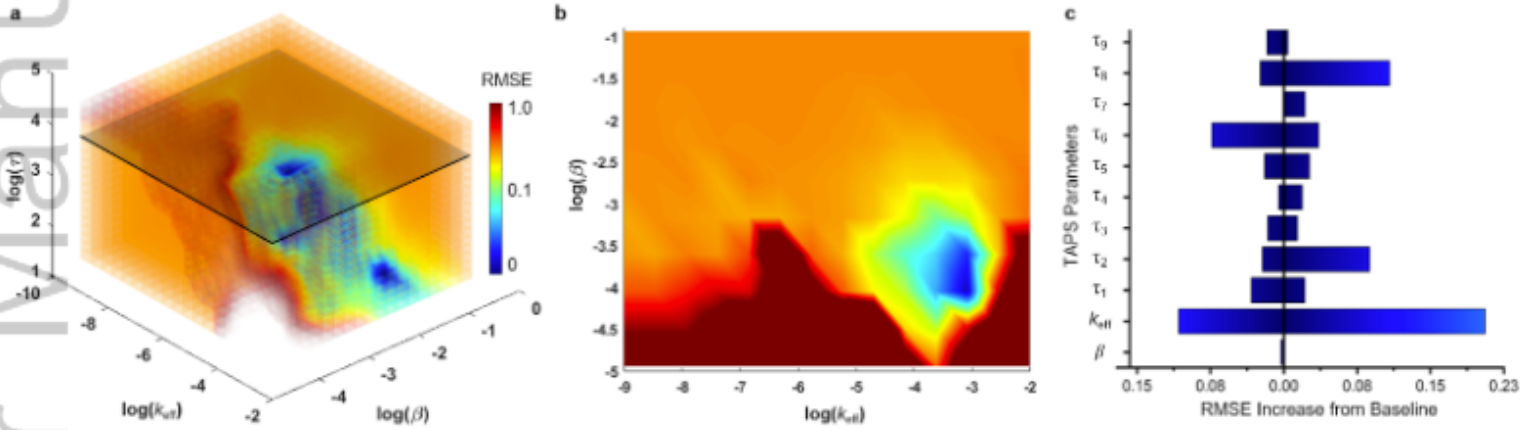


Figure5.png